An inflammatory T-cell-stromal axis contributes to hematopoietic stem/progenitor cell failure and clonal evolution in human myelodysplastic syndrome

Lanpeng Chen[1#], Yujie Bian[1#], Eline Pronk[1], Claire van Dijk[1], Tim van Tienhoven[1], Remco M. Hoogenboezem[1], Eric M. Bindels[1], Dennis Bosch[1], Sadaf Fazeli[2], Aniek O. de Graaf[3], Theresia M. Westers[4], Maksim Kholmatov[5], Judith B. Zaugg[5], Pedro L. Moura[2], Eva Hellström-Lindberg[2], Arjan A. van de Loosdrecht[4], Joop H. Jansen[3], Mathijs A. Sanders[1] and Marc H.G.P. Raaijmakers*[1]

[1] Department of Hematology, Erasmus MC Cancer Institute, Rotterdam, the Netherlands

[2] Department of Medicine Huddinge, Center for Hematology and Regenerative Medicine, Karolinska Institute, Huddinge, Sweden

[3] Laboratory of Hematology-Department of Laboratory Medicine, Radboud UMC, Nijmegen, the Netherlands

[4] Amsterdam UMC, Vrije Universiteit Amsterdam, Department of Hematology, Cancer Center Amsterdam, Amsterdam, Netherlands

[5] European Molecular Biology Laboratory, Structural and Computational Biology Unit, Heidelberg, Germany

These authors contributed equally

*Corresponding Author: Marc H.G.P. Raaijmakers, Department of Hematology, Erasmus MC Cancer Institute, Dr. Molewaterplein 40, 3015 GD Rotterdam, the Netherlands. Phone: +31-107033123; E-mail: m.h.g.raaijmakers@erasmusmc.nl

Figure S1

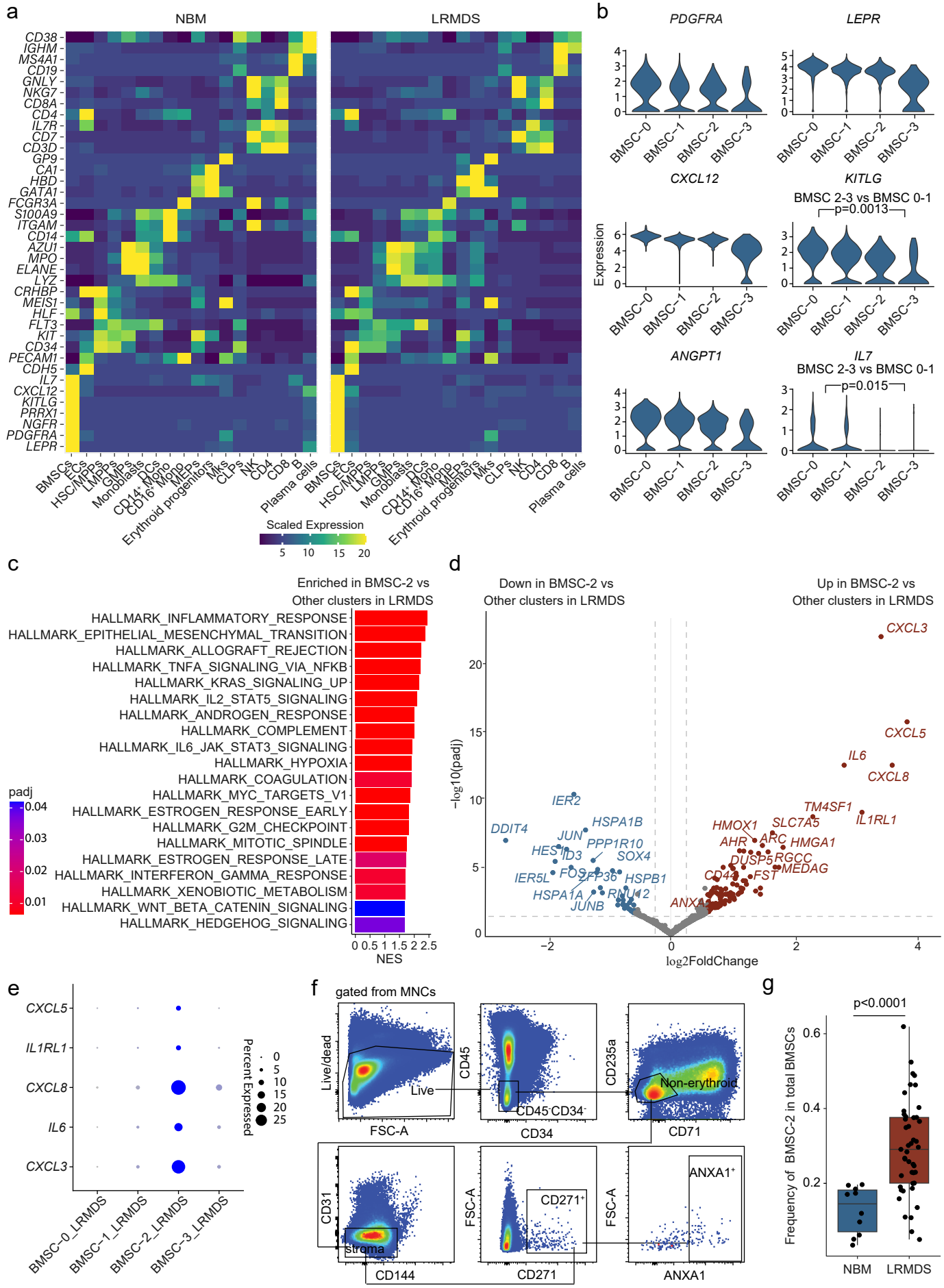


Fig. S1 Transcriptional characterization of BMSC heterogeneity in the single cell LR-MDS taxonomy (related to Figure 1 and 2)

(a) Expression of cell-identifying genes in each cell subtype in NBM and LR-MDS.
(b) Genes encoding HSPC regulatory factors *KITLG*, *ANGPT1* and *IL7* are upregulated in BMSC-0 and BMSC-1 compared to BMSC-2 and BMSC-3. Analysis was performed at sample level using the pseudoDE package. Statistical analysis was performed by a two-sided Wald test and corrected for FDR.
(c-e) Transcriptional characterization of the BMSC-2 cluster in LR-MDS demonstrating increased expression of gene signatures indicative of NFκB-associated inflammation compared to other clusters as shown by Hallmark geneset enrichment analysis (c) and differential gene expression analysis (d-e). LR-MDS (n=4), NBM (n=4). Statistical analysis was performed by a K-S test and corrected by FDR (c). Statistical analysis was performed by a two-sided Wald test and adjusted for FDR (d).
(f) FACS gating strategy for expression of Annexin A1 on stromal cells in BM aspirates (Representative plots from LR-MDS).
(g) Estimated abundancy of the inflammatory BMSC-2 subset in LR-MDS vs. NBM as assessed by cibersort deconvolution of the BMSC pseudobulk-RNAseq dataset. LR-MDS (n=45) and NBM (n=10). Statistical analysis was performed by a two-sided Wilcoxon test.

Figure S2

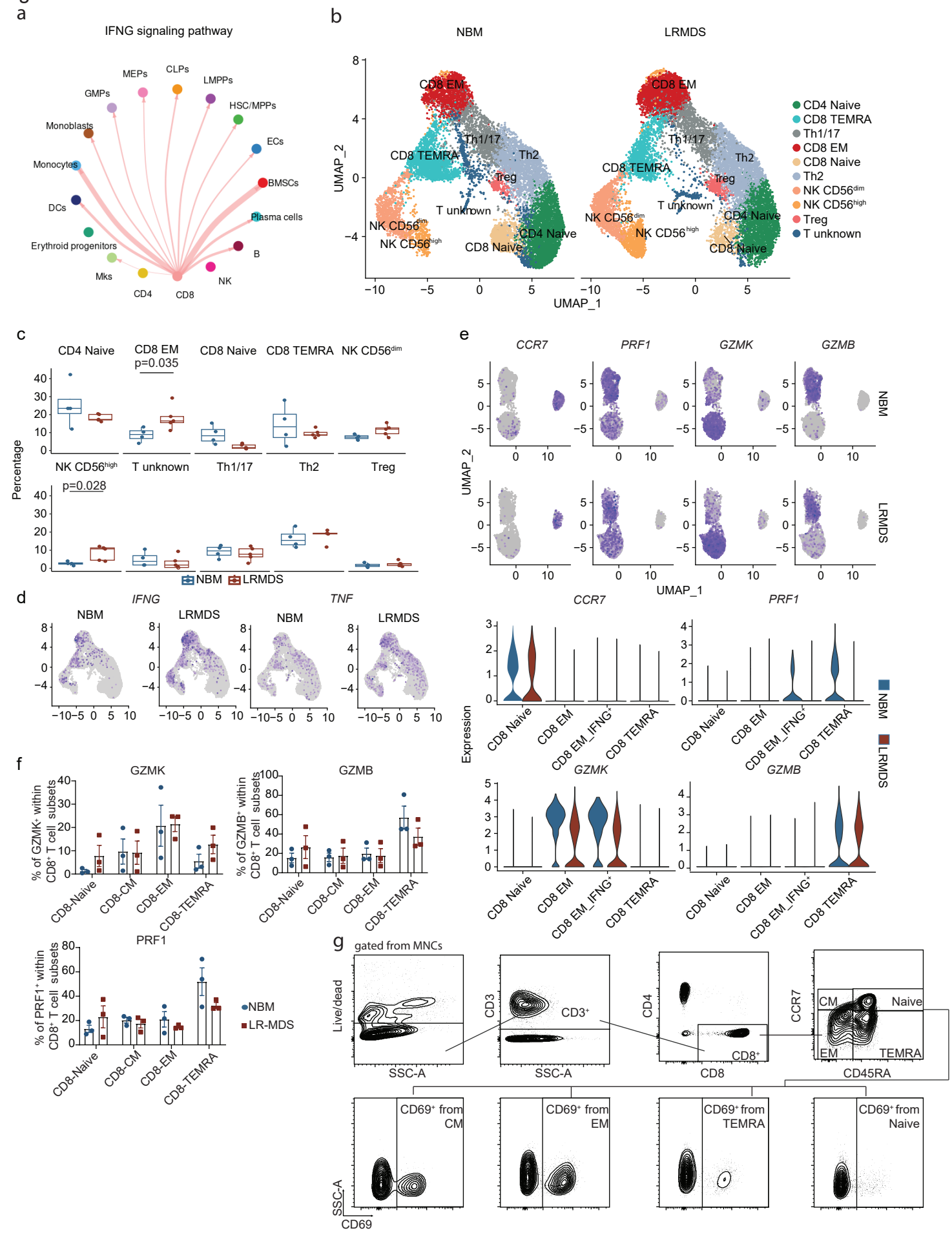


Fig. S2 Immune cells are predicted to be triggers of BMSC inflammation (related to Figure 4)

(a) CellChat ligand-receptor interaction analysis predicting that CD8⁺ T cells may be the major source of IFNγ signaling towards BMSCs in LR-MDS. (b-c) Distribution and frequency of T and NK cell subtypes in NBM (n=4) and LR-MDS (n=5) demonstrating a relative expansion of the EM CD8⁺ T cell population. Statistical analysis was performed by a two-sided unpaired Welch's t-test (c).
(d) Expression of genes encoding IFNγ and TNFα in T and NK cell subpopulations in NBM and LR-MDS.
(e) Expression of genes encoding *CCR7* (naïve marker), *Perforin-1 (PRF1)*, *Granzyme B (GZMB)* and *Granzyme K (GZMK)* in CD8⁺ T cell subsets in NBM and LR-MDS.
(f) Percentage of GZMK⁺, GZMB⁺ and Perforin-1⁺ cells within the different subsets of CD8⁺ T cells, as assessed by flow-cytometry. NBM (n=3) and LR-MDS (n=3). Error bar represents mean ± SEM.
(g) FACS gating strategy for EM population within CD8⁺ T cell, and for CD69⁺ within CD8⁺ Naive, CM, EM, TEMRA subsets.(Representative plots from NBM)

Source data are provided as a Source Data file.

Figure S3

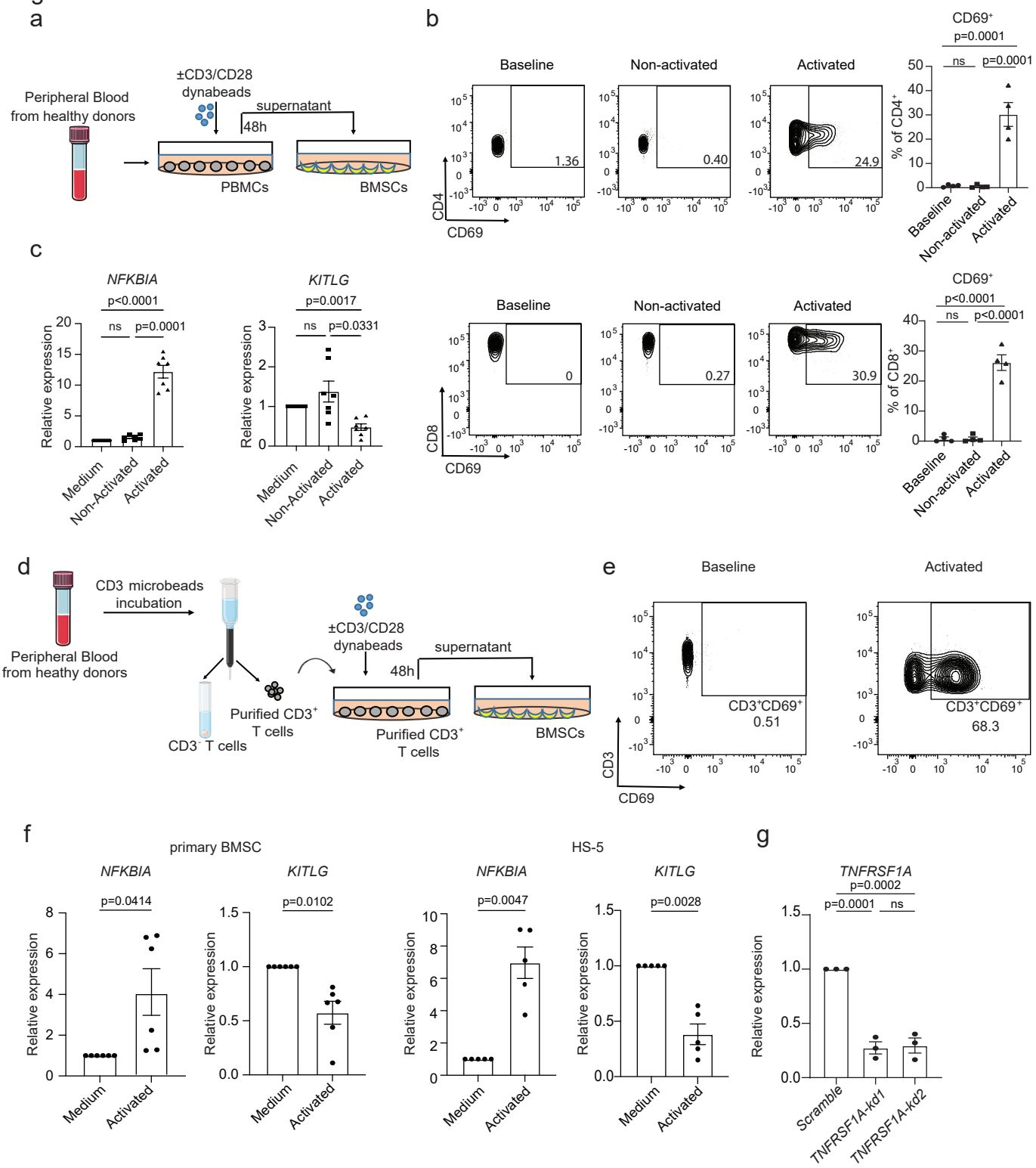


Fig. S3 Inflammatory activation of BMSCs by the secretome of activated purified T cells (related to Figure 4)

(a) Inflammatory activation of BMSCs by the secretome of activated T cells. Created in BioRender. Bian, Y. (2025) https://BioRender.com/cs43kn5. Human T cells were activated, and BMSCs were exposed to their secretome.
(b) Activation of T cells from healthy peripheral blood using CD3/CD28 dynabeads as indicated by induced expression of CD69 in CD4⁺ and CD8⁺ T cells. Baseline = T cells before activation, Non-activated = non-activated T cells, Activated = activated T cells. Statistical analysis was performed by a one-way ANOVA and Tukey's multiple comparisons test. n=4, from 4 independent experiments. ns, not significant. Error bar represents mean ± SEM.
(c) Inflammatory activation of human primary BMSCs by the secretome of activated T cells, as demonstrated by increased *NFKBIA* expression and reduced *KITLG* expression. Medium = Medium for T cells culture, Non-activated = conditional medium from non-activated T cells, Activated = conditional medium from activated T cells. Statistical analysis was performed by a one-way ANOVA and Tukey's multiple comparisons test. n=7, from 7 independent experiments. ns, not significant. Error bar represents mean ± SEM.
(d) Inflammatory activation of BMSCs by the secretome of activated CD3⁺ T cells. Created in BioRender. Bian, Y. (2025) https://BioRender.com/iu6erfi. CD3⁺ T cells in human peripheral blood were purified by CD3 microbeads and activated by CD3/CD28 dynabeads, BMSCs were exposed to their secretome.
(e) Representative FACS plot demonstrating induction expression of CD69 upon activation of CD3⁺ T cells.
(f) Induction of *NFKBIA* and reduction in *KITLG* gene expression upon T cell activation in primary BMSCs (left panels) and HS-5 cells (right panels), recapitulating aspects of stromal inflammation in LR-MDS. Primary BMSCs, n=6, from 6 independent experiments. HS-5 cells, n=5, from 5 independent experiments. Statistical analysis was performed by a two-sided paired t-test. Error bar represents mean ± SEM.
(g) Validation of knockdown efficacy of two shRNAs targeting *TNFRSF1A* in HS-5 BMSCs. Statistical analysis was performed by a one-way ANOVA and Tukey's multiple comparisons test. n=3, from 3 independent experiments. ns, not significant. Error bar represents mean ± SEM.

Source data are provided as a Source Data file.

Figure S4

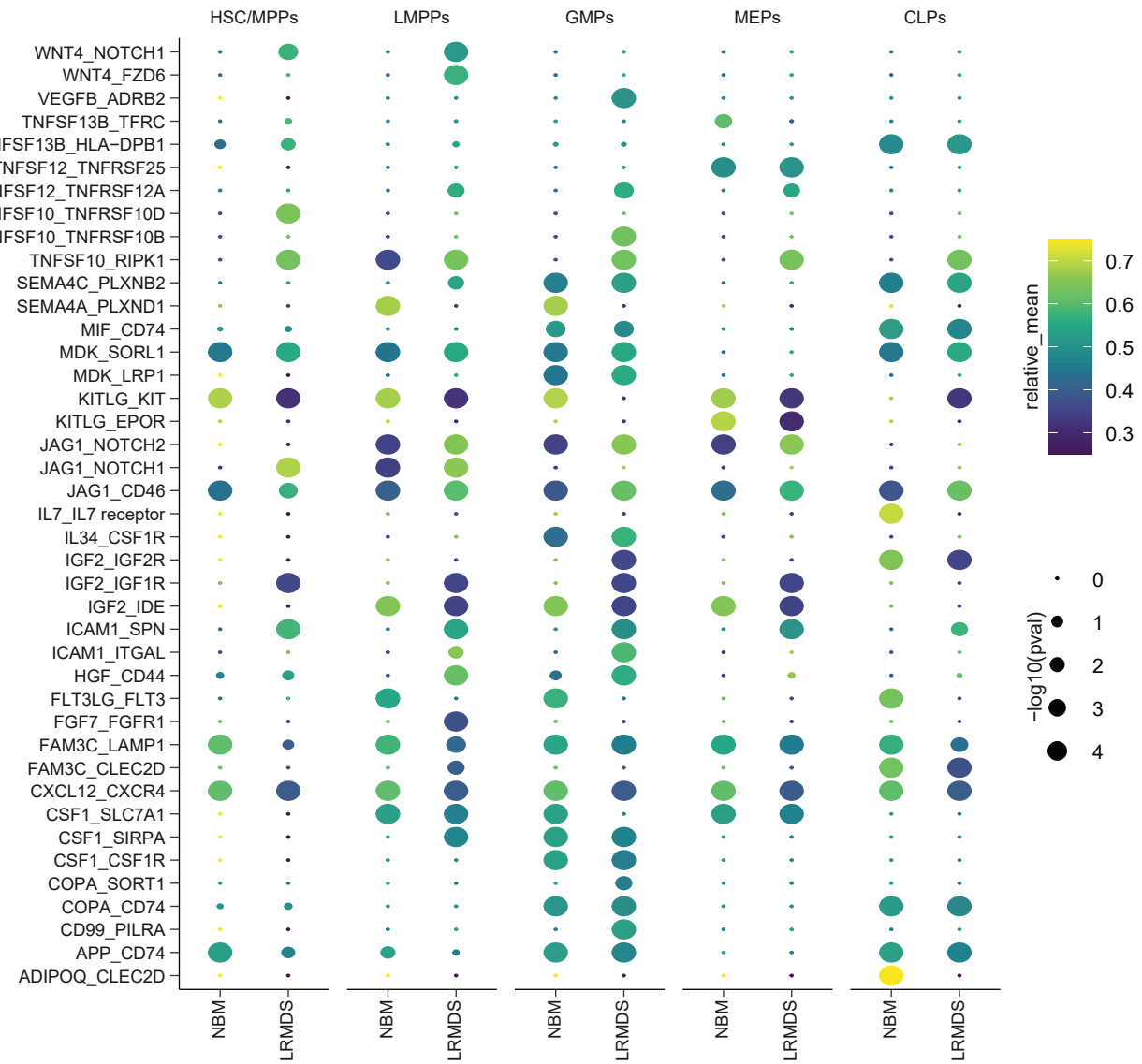


Fig.S4 Predicted interactions between BMSCs and HSPCs in NBM and LR-MDS (related to Figure 5)

Predicted relative strength of ligand-receptor signaling pathways originating from BMSCs to HSPC subtypes in NBM and LR-MDS. Color scale and dot size represent relative mean strength and p-value of interactions, respectively. CellphoneDB was used for the assessment.

Figure S5

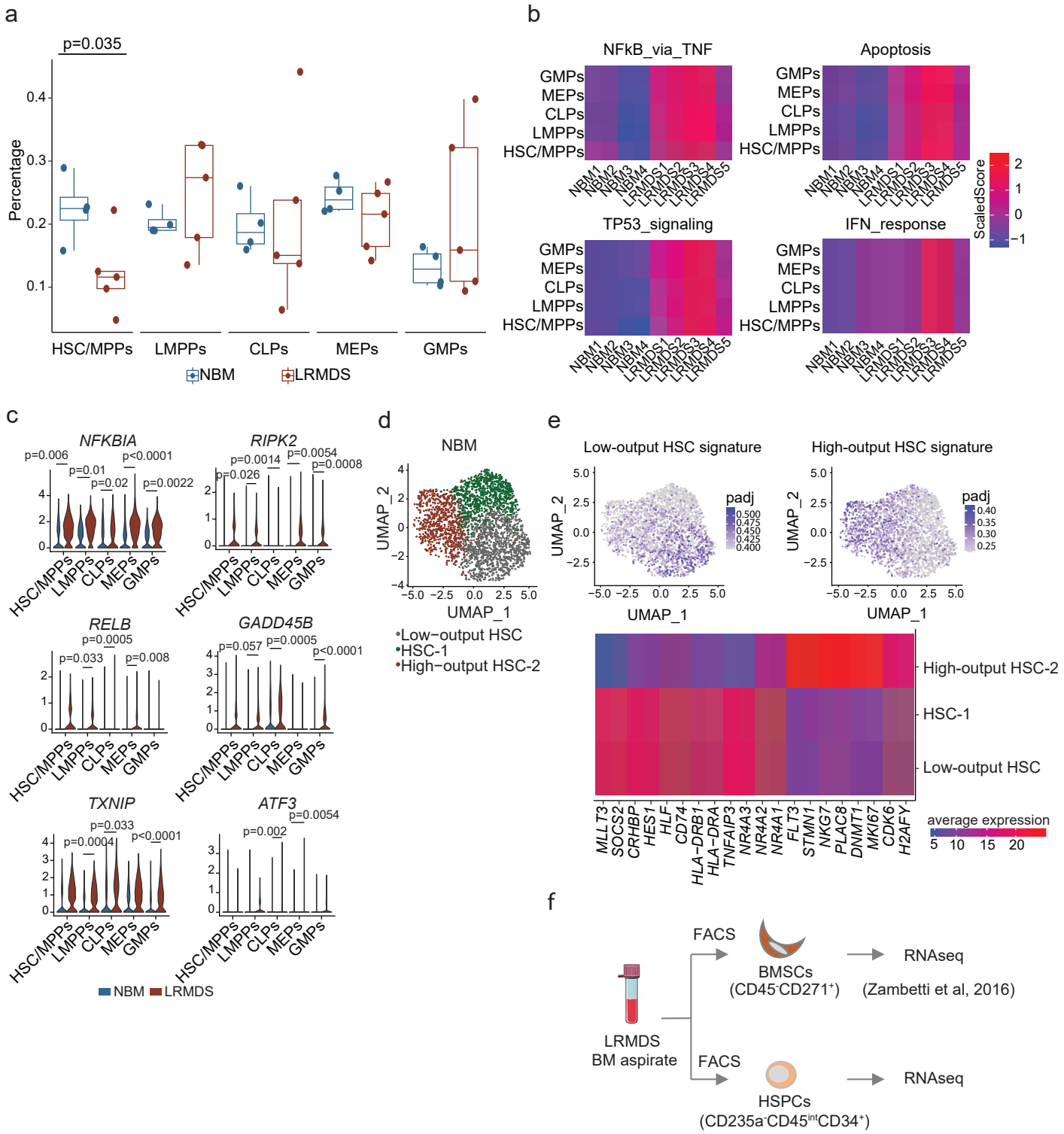


Fig. S5 HSPC composition and transcriptional changes in LR-MDS (related to Figure 5)

(a) Frequencies of HSPC subpopulations in NBM and LR-MDS. Statistical analysis was performed by a unpaired Welch's t-test. NBM (n=4) and LR-MDS (n=5). Data are presented as boxplots: the central line marks the median, the box spans the 25th to 75th percentiles (interquartile range), and whiskers extend to the smallest and largest values within 1.5× the interquartile range. Data points beyond this range are shown individually as outliers.
(b) Enrichment of Hallmark gene signatures indicative of inflammatory stress in each HSPC subpopulation across all NBM and LR-MDS samples.
(c) Expression of "*leading-edge*" genes indicative of inflammatory stress in HSPC subsets. NBM (n=4), LR-MDS (n=5). Statistical analysis was performed by a two-sided unpaired Welch's t-test. PseudoDE R-package is used for differential expression gene analysis at sample levels.
(d-e) Subclustering of the HSC/MPP population in NBM resulted in the identification of 'low-output' HSC, HSC-1 and 'high-output' HSC-2 substes. Annotation is based on enrichment of gene signatures and genes indicative of low- and high-output HSCs.
(f) Experimental design for paired bulk-RNA-seq on HSPCs ($CD45^{int}CD235a^{-}CD34^{+}$) and BMSCs in NBM (n=7) and LR-MDS (n=38). Created in BioRender. Bian, Y. (2025) https://BioRender.com/6qqnzqk.

Figure S6

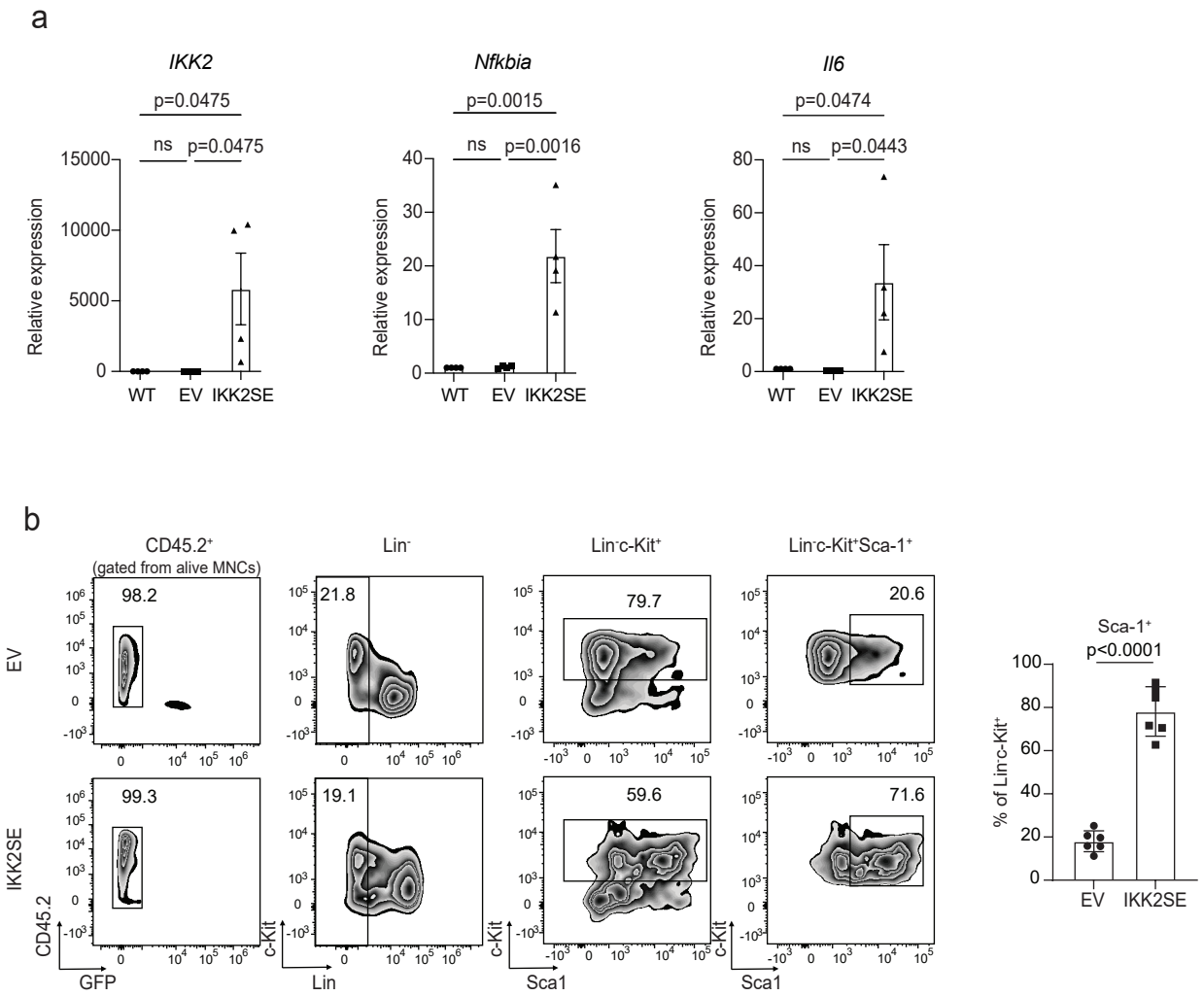


Fig. S6 Inflammatory activation of BMSCs in vitro and co-culture with HSPCs (related to Figure 6)

(a) Murine BMSCs (OP9 cells) were transduced with IKK2SE or empty vector control. Expression of *IKK2* and inflammatory markers (*Il6*, *Nfkbia*) after transduction are shown. Statistical analysis was performed by a one-way ANOVA and Tukey's multiple comparisons test. ns, not significant. n=4, from 4 independent experiments. Error bar represents mean ± SEM.
(b) Inflammatory activation of Lin$^-$ HSPCs upon culture on inflamed BMSCs as indicated by upregulation of Sca-1 expression. Representative flow cytometry plots of immunophenotype of HSPC after coculture with OP9. Statistical analysis was performed by a two-sided unpaired Welch's t-test. Error bar represents mean ± SEM. (replicates from n=2 mice performed in triplicates).

Source data are provided as a Source Data file.

Figure S7

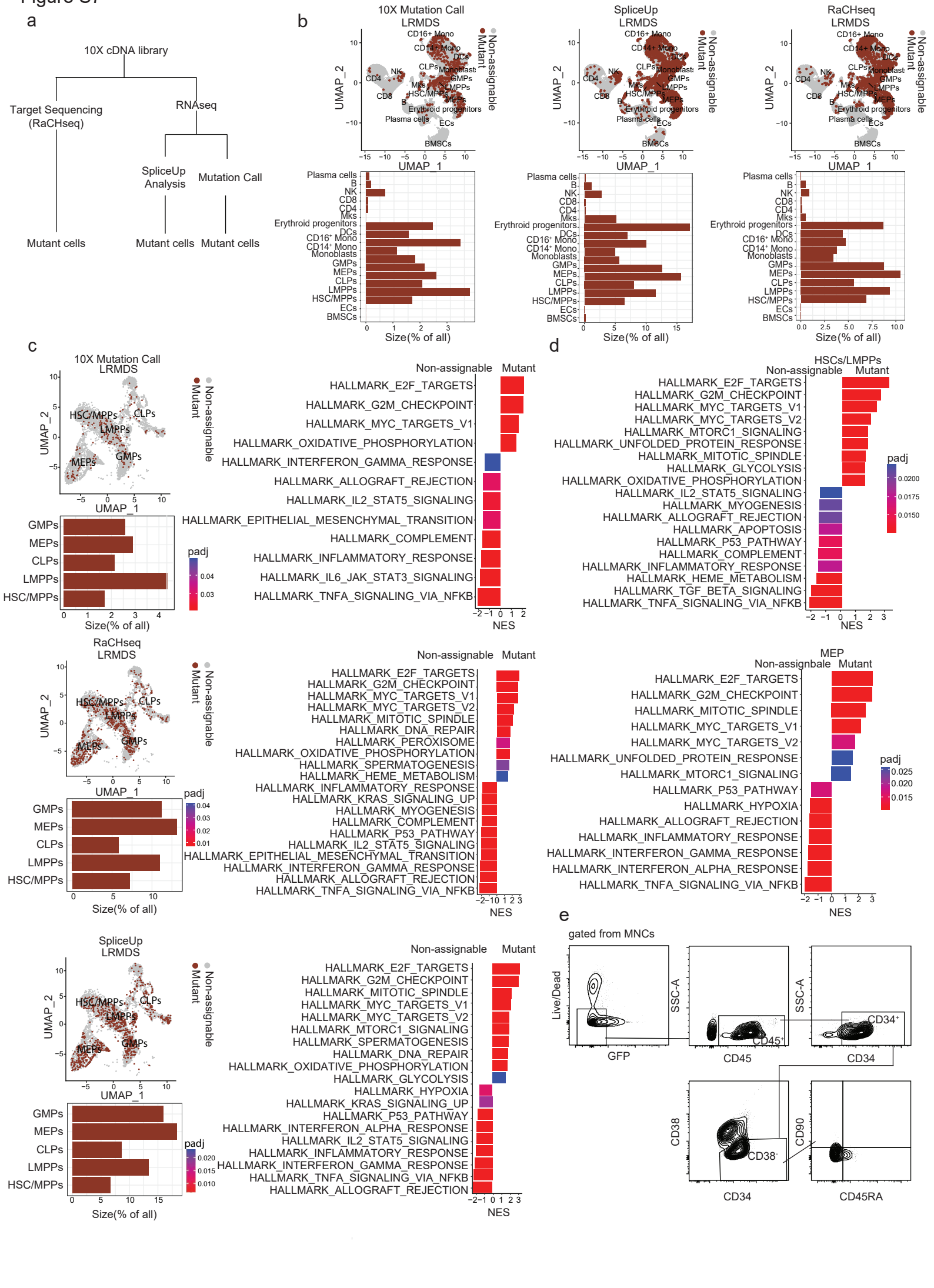
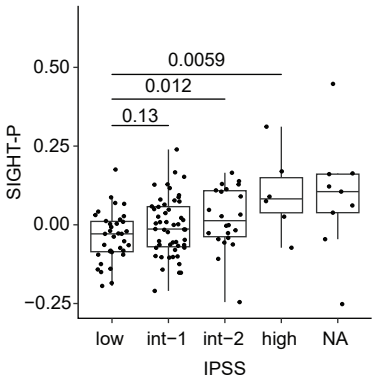

a
10X cDNA library
Target Sequencing (RaCHseq)
RNAseq
SpliceUp Analysis
Mutation Call
Mutant cells
Mutant cells
Mutant cells
b
10X Mutation Call LRMDS
SpliceUp LRMDS
RaCHseq LRMDS
Mutant
Non-assignable
UMAP_1
UMAP_2
Size(% of all)
c
d
HSCs/LMPPs
MEP
padj
NES
e
gated from MNCs
Live/Dead
GFP
SSC-A
CD45
CD34
CD38
CD90
CD45RA

Fig. S7 Detection of mutant cells in the LR-MDS taxonomy using different experimental approaches (related to Figure 7)

(a-b) Identification and distribution of mutant cells within the LR-MDS taxonomy by 10X RNA-seq mutational calling, RaCHseq and SpliceUp computational analysis, respectively.
(c) Identification and distribution of mutant cells within HSPC subsets in LR-MDS using the different methodologies, showing consistent results regarding transcriptional programs in mutant HSPCs indicating relative mitigation of inflammatory stress signaling and cell-cycle progression. Positive NES reflects programs enriched in mutant HSPCs, while negative scores indicate enrichment in non-assignable HSPCs. All cells in HSC/MPPs, LMPPs, MEPs, and GMP clusters were used in the analysis. Statistical analysis was performed by a K-S test and corrected for FDR.
(d) Differentially expressed gene programs in mutant (vs. 'non-assignable' cells) HSC/MPP and MEP subsets demonstrating consistent mitigation of inflammatory stress pathways and enrichment of gene programs implicated in cell cycle progression in these HSPC subsets. Positive NES reflects programs enriched in mutant HSPCs, while negative scores indicate enrichment in non-assignable HSPCs. Statistical analysis was performed by a K-S test and corrected for FDR.
(e) FACS gating strategy for immunophenotypic HSPCs ($CD34^+$ and $CD34^+CD38^-CD45RA^-CD90^+$) from BMSC-HSPCs cocultures. (Representative plots from NBM-IKK2SE).

Figure S8

a



b

	Leukemia Risk		
	HR	± SEM	p-value
SIGHT-P	244	2.11	0.009
Age	1.02	0.029	0.53
IPSS(vs High)			
Low	0	0.86	<0.001
Int-1	1.2	0.916	0.84
Int-2	2.54	0.838	0.27

c

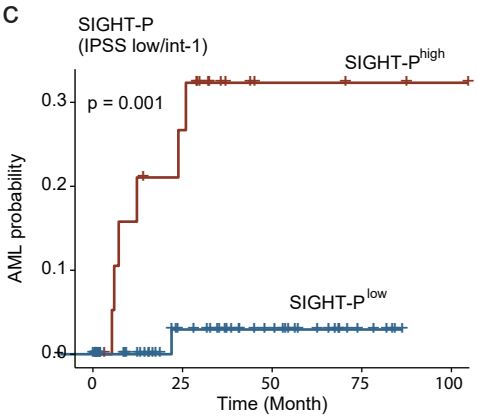


Fig. S8 Stromal inflammation is associated with outcome in LR-MDS (related to Figure 8)

(a) The level of stromal inflammation, as indicated by the SIGHT-P is associated with the International Prognostic Scoring System (IPSS) risk score in the GSE58831 cohort. A Wilcoxon rank sum test was used for statistics.
(b) Cause-specific independent prognostic value of SIGHT-P compared to IPSS and age in MDS, as assessed by competing risk regression analysis in the GSE58831 cohort.
(c) Association between SIGHT-P and leukemic progression in LR-MDS patients in the GSE58831 cohort, depicted by cumulative frequency curves. Statistical analysis was performed by a Gray's test.